BEM/FVM conjugate heat transfer analysis of a three-dimensional film cooled turbine blade

A. Kassab and E. Divo
Mechanical, Materials, and Aerospace Engineering Department, University of Central Florida, Orlando, Florida, USA
J. Heidmann
James D. Heidmann, NASA Glenn Research Center, Cleveland, Ohio, USA
E. Steinthorsson
A&E Consulting, 27563 Hemlock Drive, Westlake, Ohio, USA
F. Rodriguez
Mechanical, Materials, and Aerospace Engineering Department, University of Central Florida, Orlando, Florida, USA

Received July 2002
Revised January 2003
Accepted January 2003

Keywords *Heat transfer, Coupled phenomena, Boundary elements, Finite volume*

Abstract *We report on the progress in the development and application of a coupled boundary element/finite volume method temperature-forward/flux-back algorithm developed to solve conjugate heat transfer arising in 3D film-cooled turbine blades. We adopt a loosely coupled strategy where each set of field equations is solved to provide boundary conditions for the other. Iteration is carried out until interfacial continuity of temperature and heat flux is enforced. The NASA-Glenn explicit finite volume Navier-Stokes code Glenn-HT is coupled to a 3D BEM steady-state heat conduction solver. Results from a CHT simulation of a 3D film-cooled blade section are compared with those obtained from the standard two temperature model, revealing that a significant difference in the level and distribution of metal temperatures is found between the two. Finally, current developments of an iterative strategy accommodating large numbers of unknowns by a domain decomposition approach is presented. An iterative scheme is developed along with a physically-based initial guess and a coarse grid solution to provide a good starting point for the iteration. Results from a 3D simulation show the process that converges efficiently and offers substantial computational and storage savings.*

1. Introduction

Engineering analysis of complex mechanical devices such as turbomachines requires an ever-increasing fidelity in numerical models upon which designers

This research was carried out under the funding from an NRA grant NAG3-2311 from NASA Glenn Research Center. The authors are grateful to Dr Ali Ameri of AYT corporation for his helpful input and advice in the course of this study.

International Journal of Numerical Methods for Heat & Fluid Flow
Vol. 13 No. 5, 2003
pp. 581-610

0961-5539
DOI 10.1108/09615530310482463

rely in their efforts to attain demanding specifications placed on the efficiency and durability of modern machinery. Consequently, the trend in computational mechanics is to adopt coupled-field analysis to obtain computational models, which attempt to better mimic the physics under consideration (Kassab and Aliabadi, 2001). The coupled-field problem, which we address in this paper is conjugate heat transfer (CHT), i.e. the coupling of convective heat transfer external to the solid body of a thermal component coupled to conduction heat transfer within the solid body of that component (Figure 1). CHT thus applies to any thermal system in which the multi-mode convective/conduction heat transfer is of particular importance to thermal design, and thus CHT in most instances arises naturally where the external and internal temperature fields are coupled.

Conjugacy is often ignored in most analytical solutions and numerical simulations. For instance, it is in common practice in the analysis of turbomachinery (Heidmann *et al.*, 2002) to carry out separate flow and heat conduction analyses. Heat transfer coefficient as well as film effectiveness values are predicted using two independent external flow solutions, each computed by imposing a different constant wall temperature at the surfaces of the turbine blade exposed to hot gases and film cooling air. The film effectiveness determines the reference temperature for the computed film coefficients. In turn, these values are used to impose convective boundary conditions to a conduction solver to obtain predicted metal temperatures. As shown in the example section of this paper, the shortcomings of this approach, which neglects the effects of the wall temperature distribution on the development of the thermal boundary layer are readily overcome by a CHT analysis, in which the coupled nature of the field problem is explicitly taken into account in the analysis.

There are two basic approaches to solve the coupled field problems. In the first approach, a direct coupling is implemented in which different fields are solved simultaneously in one large set of equations. Direct coupling is mostly applicable for problems where time accuracy is critical, for instance, in aero-elasticity applications where the timescale of the fluid motion is of the same order as the structural modal frequency. However, this approach suffers a major disadvantage due to mismatch in the structure of the coefficient matrices arising from boundary element method (BEM), finite element method (FEM) and/or finite volume method (FVM) solvers. That is, given the fully populated nature of the BEM coefficient matrix, the direct coupling approach would

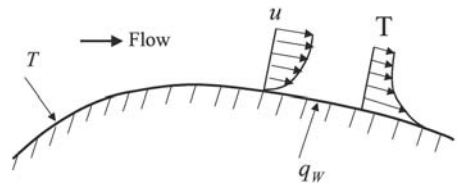

Figure 1.
CHT problem: external convective heat transfer coupled to heat conduction within the solid

severely degrade the numerical efficiency of the solution by directly incorporating the fully populated BEM equations into the sparsely banded FEM or FVM equations. A second approach which may be followed is a loose coupling strategy where each set of field equations is solved separately to produce boundary conditions for the other. The equations are solved in turn until an iterated convergence criterion, namely continuity of temperature and heat flux, is met at the fluid-solid interface. The loose coupling strategy is particularly attractive when coupling auxiliary field equations to computational fluid dynamics codes as the structure of neither solver interferes in the solution process.

Several approaches can be taken to solve the coupled field problems and are mostly based on either FEM or FVM or a combination of these two field solvers. Examples of such loosely coupled approaches applied to a variety of CHT problems ranging from engine block models to turbomachinery can be found in Bohn *et al.* (1997, 1999), Comini *et al.* (1993), Hahn *et al.* (2000), Kao and Liou (1997), Patankar (1978), Shyy and Burke (1994), and in Tayala *et al.* (2000) where multi-disciplinary optimization is considered for CHT modelled turbine airfoil designs. Hassan *et al.* (1998) developed a conjugate algorithm, which loosely couples a FVM-based hypersonic CFD code to an FEM heat conduction solver in an effort to predict ablation profiles in hypersonic re-entry vehicles. Here, the structured grid of the flow solver is interfaced with the unstructured grid of heat conduction solvers in a quasi-transient CHT solution tracing the re-entry vehicle trajectory. Issues in loosely coupled analysis of the elastic response of the solid structures perturbed by the external flowfields arising in aero-elastic problems can be found in Brown (1997) and Dowell and Hall (2001). In either case, the coupled field solution requires complete meshing of both fluid and solid regions while enforcing solid/fluid interface continuity of fluxes and temperatures, in the case of CHT analysis, or displacement and traction, in the case of aero-elasticity analysis.

A different approach was taken by Li and Kassab (1994a, b) and Ye *et al.* (1998), to develop a BEM-based CHT algorithm thereby avoiding meshing of the solid region for the conduction solution. The method couples the BEM to a FVM Navier-Stokes solver and was applied to solve the two-dimensional steady-state compressible subsonic CHT problems over the cooled and uncooled turbine blades. The conduction problem requires solution of the Laplace equation for the temperature (or the Kirchhoff transform in the case of temperature dependent conductivity), and, as such, only requires a boundary discretization thereby eliminating the onerous task of grid generation within the intricate regions of the solid. The boundary discretization utilized to generate the computational grid for the external flow-field can be considerably coarsened to provide the boundary discretization required for the BEM. Most modern grid generators used in the computational fluid dynamics, for instance, GridPro™ (Program Development Corporation, 1997), the topology-based

algebraic grid generator used in the examples presented in this paper, allow the multigrid option. Several levels of coarse discretization can thus be readily obtained. Furthermore, the BEM/FVM methods offer the additional advantage of providing heat flux values and this stems from the fact that nodal unknowns which appear in the BEM are the surface temperatures and heat fluxes. Consequently, solid/fluid interfacial heat fluxes that are required to enforce continuity in the CHT problems are naturally provided by the BEM conduction analysis. This is in sharp contrast to the domain meshing methods, such as FVM and FEM where heat fluxes are computed by the numerical differentiation in a post-processing stage. He *et al.* (1995a, b) adopted the BEM/FVM approach in the further studies of CHT in incompressible flow in ducts subjected to a constant wall temperature and constant heat flux boundary conditions. Kontinos (1997) also adopted the BEM/FVM coupling algorithm to solve the CHT over metallic thermal protection panels at the leading edge of the X-33 in a Mach 15 hypersonic flow regime. Rahaim *et al.* (1997, 2000) adopted a BEM/FVM strategy to solve the time-accurate CHT problems for supersonic compressible flow over a 2D wedged, and they present experimental validation of this CHT solver. In their studies, the dual reciprocity BEM (Partridge *et al.*, 1992) was used for transient heat conduction, while a cell-centered FVM was chosen to resolve the compressible turbulent Navier-Stokes equations.

In this paper, we report on the progress in the development and application of a BEM-based temperature forward/flux back (TFFB) coupling algorithm developed to solve the CHT arising in the 3D film-cooled turbine blades. The NASA-Glenn turbomachinery Navier-Stokes code Glenn-HT is coupled to a 3D BEM steady-state heat conduction solver. The steady-state solution is sought by marching in time until dependent variables reach their steady-state values, and, as such, intermediate temporal solutions are not physically meaningful. In this mode of solving the steady-state problem, time-marching can be viewed as a relaxation scheme, and local time-stepping and implicit residual smoothing are used to accelerate convergence. The steady heat conduction equation reduces to the Laplace equation, and it is solved using the BEM with isoparametric bilinear discontinuous elements. We chose to employ discontinuous elements as they provide high levels of accuracy in computed heat flux values especially at sharp corner regions where first kind boundary conditions are imposed without resorting to special treatment of corner points required by continuous elements in particular, when first kind boundary conditions are imposed (Kane, 1994; Kassab and Nordlund, 1994). In this application, sharp corners occur in many locations and first kind boundary conditions are imposed on all metal surfaces. Moreover, the use of discontinuous elements throughout the BEM model eliminates much of the overhead associated with continuous elements, in particular, there is no need to generate, store, or access a connectivity matrix when using the discontinuous elements.

In order to resolve the flow physics, the CFD grid must be clustered in many regions. The BEM grid does not require such fine clustering and consequently, the two grids are of quite different coarsenesses. The details of the interpolation used to exchange nodal temperature and flux information from the disparate CFD and BEM grids are presented. Results from a CHT numerical simulation of a 3D film-cooled blade section are presented and results are compared with those obtained from the standard approach of a two-temperature model. Significant difference in the level and distribution of the metal temperature is found between the two-temperature and CHT models. Finally, in order to address the large number of unknowns appearing in the 3D BEM model, current developments of a strategy of artificial subsectioning of the blade are presented. Here, the approach is to subsection the blade in the spanwise direction. A specially tailored iterative scheme is developed to solve the conduction problem with each subsection BEM problem solved using a direct LU solver. A physically based initial guess is used to provide a good starting point for the iterative algorithm. Results from the 2D and 3D simulations show the process converging efficiently and offers a substantial computational and storage savings.

2. Governing equations

We first present the governing equations for the coupled field problem under consideration. The CHT problems arising in turbomachinery involves external flow-fields that are generally compressible and turbulent, and these are governed by the compressible Navier-Stokes equations supplemented by a turbulence model. Heat transfer within the blade is governed by the heat conduction equation. Linear as well as non-linear options are considered. However, fluid flows within the internal structures to the blade, such as film cooling holes and channels, are usually of low-speed and are incompressible. Consequently, density-based compressible codes tend to experience numerical difficulties in modeling such flows, unless low Mach number pre-conditioning is implemented (Turkel, 1987, 1993). The Glenn-HT code is specialized to turbomachinery applications for which air is the working fluid and is modelled as an ideal gas.

2.1 Governing equations for the flow-field

The governing equations for the flow-field are the compressible Navier-Stokes equations, which describe the conservation of mass, momentum and energy. These can be written in integral form as

$$\int_{\Omega} \frac{\partial \underset{\sim}{W}}{\partial t} \, d\Omega + \int_{\Gamma} (\underset{\sim}{F} - \underset{\sim}{T}) \cdot \hat{n} \, d\Gamma = \int_{\Omega} \underset{\sim}{S} \, d\Omega \tag{1}$$

where Ω denotes the volume, Γ denotes the surface bounded by the volume Ω, and $\hat{n}$ is the outward-drawn normal. The conserved variables are contained in the vector $\underset{\sim}{W} = (\rho, \rho u, \rho v, \rho w, \rho e, \rho k, \rho\omega)$, where, ρ, u, v, w, e, k, ω are the density, the velocity components in x-, y-, and z-directions, and the specific total energy. The kinetic energy of turbulent fluctuations is denoted by k and the specific dissipation rate is denoted by ω and both appear in the two equation – Wilcox turbulence model (Wilcox, 1993, 1994) with modifications by Menter (1993) and Chima (1996) as implemented in Glenn-HT. The vectors $\underset{\sim}{F}$ and $\underset{\sim}{T}$ are convective and diffusive fluxes, respectively, $\underset{\sim}{S}$ is a vector containing all terms arising from the use of a non-inertial reference frame as well as in the production and dissipation of turbulent quantities. The working fluid is air, and it is modeled as an ideal gas. A rotating frame of reference can be adopted for the modeling of rotating flows. The effective viscosity is given by

$$\mu = \mu_l + \mu_t \tag{2}$$

where $\mu_t = \rho k/\omega$. The thermal conductivity of the fluid is then computed by a Prandtl number analogy where

$$k_f = \frac{\gamma}{\gamma - 1}\left[\frac{\mu_l}{\mathrm{Pr}_l} + \frac{\mu_t}{\mathrm{Pr}_t}\right] \tag{3}$$

where Pr is the Prandtl number and γ is the specific heat ratio. The subscripts l and t refer to laminar and turbulent values, respectively.

2.2 The governing equations of the heat conduction field

In the steady-state CHT solutions obtained in this paper, the NS equations are solved to steady-state by a time marching scheme converging towards steady-state. A steady heat conduction analysis is carried out using the BEM at each time level chosen for the external flow-field and internal conduction field to interact in the iterative process. As such, the governing equation under consideration is

$$\nabla \cdot [k(T_\mathrm{s})\nabla T_\mathrm{s}] = 0 \tag{4}$$

where T_s denotes the temperature of the solid, and k_s is the thermal conductivity of the solid material. If the thermal conductivity is taken as constant, then the above equation reduces to the Laplace equation for the temperature. When the thermal conductivity variation with temperature is an important concern, the nonlinearity in the steady-state heat conduction equation can readily be removed by introducing the classical Kirchhoff transform, $U(T)$ (Azevedo and Wrobel, 1988; Bialecki and Nhalik, 1989; Kassab and Wrobel, 2000), which is defined as

$$U(T) = \frac{1}{k_o}\int_{T_o}^{T} k_s(T)\,\mathrm{dT} \tag{5}$$

where T_o is the reference temperature and k_o is the reference thermal conductivity. The transform and its inverse are readily evaluated, either analytically or numerically, and the heat conduction equation transforms to a Laplace equation for the transform parameter $U(T)$. The heat conduction equation thus reduces to the Laplace equation in any case, and this equation is readily solved by the BEM.

In the conjugate problem, continuity of temperature and heat flux at the blade surface, Γ, must be satisfied:

$$T_f = T_s$$
$$k_f \frac{\partial T_f}{\partial n} = -k_s \frac{\partial T_s}{\partial n} \tag{6}$$

Here, T_f is the temperature computed from the N-S solution, T_s is the temperature within the solid which is computed from the BEM solution, and $\partial/\partial n$ denotes the normal derivative. Both first kind and second kind boundary conditions transform linearly in the case of temperature-dependent conductivity. In such a case, the fluid temperature is used to evaluate the Kirchhoff transform and this used a boundary condition of the first kind for the BEM conduction solution in the solid. Subsequently, the computed heat flux, in terms of U, is scaled to provide the heat flux which is in turn used as an input boundary condition for the flow-field.

3. Field solver solution algorithms

A brief description of the Glenn-HT code is given in this section. Details of the code and its verification in turbomachinery application can be found in Ameri *et al.* (1997), Heidmann *et al.* (2002), Rigby *et al.* (1997), Steinthorsson *et al.* (n.d., 1993). The heat conduction equation is solved using the BEM.

3.1 Navier-Stokes solver

Glenn-HT uses a cell-centered FVM to discretize the NS equations. Equation (1), is integrated over a hexahedral computational cell with the nodal unknowns located at the cell center (i, j, k). The convective flux vector is discretized by a central difference supplemented by artificial dissipation as described in Jameson *et al.* (1981). The artificial dissipation is a blend of first and third order differences with the third order term active everywhere except at shocks and locations of strong pressure gradients. The viscous terms are evaluated using central differences. The overall accuracy of the code is second order (Heidmann *et al.,* 2002). The resulting finite volume equations can be written at every computational node as

$$V_{i,j,k} \frac{\mathrm{d}\bar{\underset{\sim}{W}}_{i,j,k}}{\mathrm{d}t} + \underset{\sim}{q}_{i,j,k} - \underset{\sim}{d}_{i,j,k} = \underset{\sim}{s}_{i,j,k} \tag{7}$$

where $\bar{\underset{\sim}{W}}_{i,j,k}$ is the cell-volume averaged vector of conserved variables, $\underset{\sim}{q}_{i,j,k}$ and $\underset{\sim}{d}_{i,j,k}$ are the net flux and dissipation for the finite volume obtained by the surface integration of equation (1), and $\underset{\sim}{s}_{i,j,k}$ is the net finite source term. The above is solved using a time marching scheme based on a fourth order explicit Runge-Kutta time-stepping algorithm. The steady-state solution is sought by marching in time until the dependent variables reach their steady-state values, and, as such, intermediate temporal solutions are not physically meaningful. In this mode of solving the steady-state problem, time-marching can be viewed as a relaxation scheme, and local time-stepping and implicit residual smoothing are used to accelerate convergence. A multigrid option is available in the code. The code also adopts a multi-block strategy to model complex geometries associated with the film-cooled blade problems. Here, locally structured grid blocks are generated into a globally unstructured assembly.

Glenn-HT adopts a k-ω turbulence model, which integrates to the wall and does not require maintaining a specified distance from the wall, as no wall functions are used. The computational grid is sufficiently fine near the wall to yield a y^+ value of less than 1.0 at the first grid point away from the wall. A constant value of 0.9 is taken for the turbulent Prandlt number in all heat transfer computations, while a constant value of 0.72 is used for the laminar Prandtl number. Moreover, the temperature variation of the laminar viscosity is taken as a 0.7 power law (Schlichting, 1979), and c_p is taken as constant.

3.2 Heat conduction boundary element solution

The heat conduction equation reduces to the same governing Laplace equation in the temperature or the Kirchhoff transform. In the boundary element method, this governing partial differential equation is converted into a boundary integral equation (BIE) (Banerjee, 1994; Brebbia and Dominguez, 1989; Brebbia *et al.*, 1984), as

$$C(\xi)T(\xi) + \oint_S T(x)q^*(x,\xi)\,\mathrm{d}S(x) = \oint_S q(x)T^*(x,\xi)\,\mathrm{d}S(x) \tag{8}$$

where $S(x)$ is the surface bounding the domain of interest, ξ is the source point, x is the field point, $q(x) = -k\,\partial T/\partial n$ is the heat flux, $T^*(x, \xi)$ is the so-called fundamental solution, and $q^*(x, \xi)$ is its normal derivative with $\partial/\partial n$ denoting the normal derivative with respect to the outward-drawn normal. The fundamental solution (or Green free space solution) is the response of the adjoint governing differential operator at any field point x due to perturbation of a Dirac delta function acting at the source point ξ. In our case, since the steady-state heat conduction equation is self-adjoint, we have

$$k\nabla^2 T^*(x,\xi) = -\delta(x,\xi) \tag{9}$$

Solution to this equation can be found by several means, see for instance Kellogg (1953), Liggett and Liu (1983) and Morse and Feshbach (1953), as

$$T^*(x,\xi) = \frac{1}{4\pi k r(x,\xi)} \quad \text{in 3D} \tag{10}$$

where $r(x, \xi)$ is the Euclidean distance from the source point ξ. The free term $C(\xi)$ can be shown analytically to be:

$$C(\xi) = \oint_{S(x)} -k\left[\frac{\partial T^*(x,\xi)}{\partial n}\right] \mathrm{d}S(x).$$

Moreover, introducing the definition of the fundamental solution in the above equation, it can be readily determined that, in 3D, $C(\xi)$ is the internal angle (in steradians) subtended at source point divided by 4π when the source point ξ is on the boundary and takes on a value of one when the source point ξ is at the interior.

In the standard BEM, the BIE is discretized using two levels of discretization: Firstly, the surface S is discretized into a series of $j = 1, 2, \ldots, N$ elements ΔS_j, traditionally accomplished using polynomial interpolation, bilinear and biquadratic being the most common, and secondly, the distribution of the temperature and heat flux is modeled on the surface, and this is usually accomplished using the polynomial interpolation as well. It is noted that the order of discretization of the temperature and heat flux need not be same as that used for the geometry, leading to subparametric (lower order than that used for the geometry), isoparametric (same order than that used for the geometry), and superparametric (higher order than that used for the geometry) discretizations. Moreover, the temperature and heat flux are discretized using $k = 1, 2, \ldots, NPE$ number of nodal points per element whose location within the element j can be chosen to coincide with the location of the geometric nodes leading to continuous elements or to be located offset from the geometric nodes leading to discontinuous elements. We chose to employ the bilinear discontinuous isoparametric elements as they provide high levels of accuracy in computed heat flux values, especially at sharp corner regions where first kind boundary conditions are imposed without resorting to special treatment of corner points required by continuous elements (Kane, 1994; Kassab and Nordlund, 1994). In this type of boundary element, the field variables T and q are modeled with discontinuous bilinear shape functions across each element, while the geometry is represented locally as continuous bilinear surfaces. We also employed constant elements for the coarse grid solution as will be discussed later (Figure 2).

The discretized BIE is collocated at each of the boundary nodes ξ_i and there results

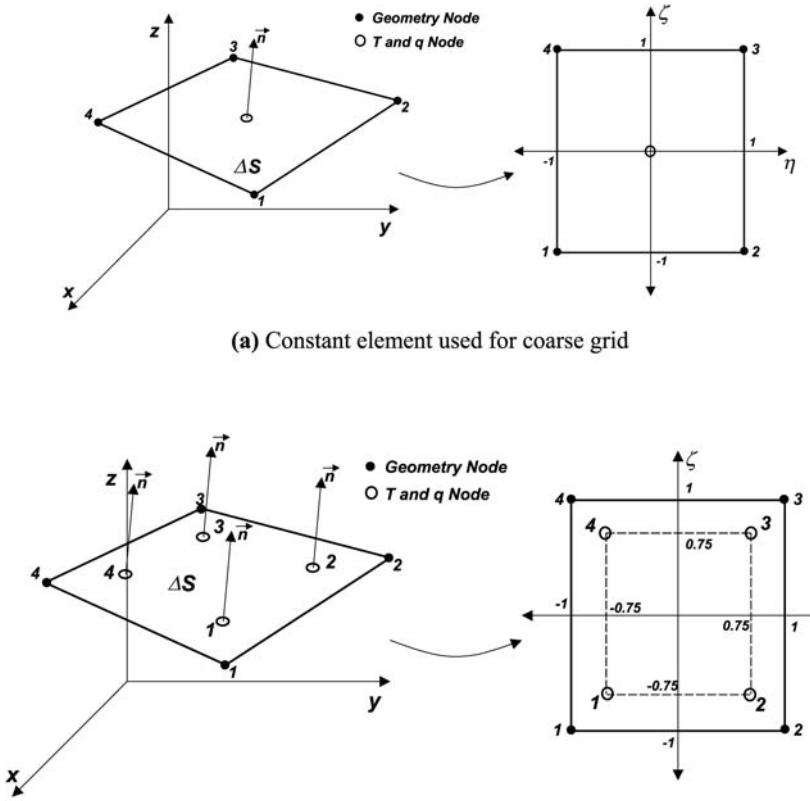

(a) Constant element used for coarse grid

(b) Discontinuous bi-linear element used in fine grid

Figure 2.
Constant and bilinear isoparameteric discontinuous boundary elements used in analysis

$$C(\xi_i)T(\xi_i) + \sum_{j=1}^{N}\sum_{k=1}^{NPE} H_{ij}^{k} T_{j}^{k} = \sum_{j=1}^{N}\sum_{k=1}^{NPE} G_{ij}^{k} q_{j}^{k} \tag{11}$$

where

$$H_{ij}^{k} = \oint_{\Delta S_j} q^{*}(x, \xi_i) M^{k}(\eta, \zeta)\, \mathrm{d}S(x)$$

and

$$G_{ij}^{k} = \oint_{\Delta S_j} T^{*}(x, \xi_i) M^{k}(\eta, \zeta)\, \mathrm{d}S(x)$$

are evaluated numerically via Gauss-Legendre quadratures with special adaption when evaluating the integrals on ΔS_i and heuristic adaptive

quadratures for elements that are close to the node of interest, and $M^k(\eta, \zeta)$ are the discontinuous shape functions used to model T and q, whose nodes located at an off-set position of 12.5 percent from the edges of the element. Upon assembly of the collocated BIEs, the following algebraic form is obtained:

$$[H]\{T_s\} = [G]\{q_s\} \tag{12}$$

Here the influence matrices $[H]$ and $[G]$ are evaluated numerically using quadratures. Once the boundary conditions are specified, the above is re-arranged in the standard form $[A]\{x\} = \{b\}$, and the ensuing equations are solved by direct or iterative methods. In a fully conjugate solution using the algorithm described in this paper, these BEM equations are solved subject to the following boundary condition at external and internal bounding walls, which are in contact with the fluid and denoted by $\Gamma_{\text{conjugate}}$:

$$T_s|_{\Gamma_{\text{conjugate}}} = T_f \tag{13}$$

In the reduced periodic 3D computational model to be discussed in the example section, adiabatic conditions are also imposed at the flowfield periodic surfaces in the spanwise direction, i.e. there

$$q_s = 0 \tag{14}$$

Once these equations are solved, the heat flux is known at all surface nodes. This is the sought-after quantity in the CHT algorithm to be shortly outlined. In the case, where the conduction problem is solved without further treatment, the basic BEM code had options of using an LU decomposition for small numbers of equations and a GMRES iterative solver with an incomplete LU (ILU) pre-conditioning for large numbers of equations. When the number of equations gets very large, storage becomes an important issue, as the coefficient matrix is fully-populated. We will discuss an effective treatment of such problems in a later section.

3.3 CHT algorithm

The Navier-Stokes equations for the external fluid flow and the heat conduction equation for heat conduction within the solid are interactively solved to steady-state through a time-marching algorithm. The surface temperature obtained from the solution of the Navier-Stokes equations is used as the boundary condition of the BEM for the calculation of heat flux through the solid surface. This heat flux is in turn used as a boundary condition for the Navier-Stokes equations in the next time-step. This procedure is repeated until a steady-state solution is obtained. In practice, the BEM is solved at every few cycles of the FVM to update the boundary conditions, as intermediate solutions are not physical in this scheme. In the calculations carried out in this study,

BEM solution was run for every ten cycles of the finite volume solver. This is referred to as the TFFB coupling algorithm as outlined below:

(1) FVM Navier-Stokes solver:
   - begins with initial adiabatic boundary condition at solid surface;
   - solves compressible NS for fluid region;
   - provides temperature distribution to the BEM conduction solver after a number of iterations;
   - receives flux boundary condition from the BEM as input for next set of iterations.

(2) BEM conduction solver:
   - receives temperature distribution from the FVM solver;
   - solves steady-state conduction problem;
   - provides flux distribution to the FVM solver.

The transfer of heat flux from the BEM to the FVM solver is accomplished as

$$q = \beta q_{\text{old}}^{\text{BEM}} + (1 - \beta) q_{\text{new}}^{\text{BEM}} \tag{15}$$

with an under-relaxation is used setting the parameter β as 0.2 in all reported calculations. The choice of the relaxation parameter is through trial and error. In certain cases, it has been our experience that a choice of larger relaxation parameter can lead to nonconvergent solutions (Bialecki *et al.*, 2001). The process is continued until the NS solver converges and wall temperatures and heat fluxes converge, i.e. until equation (6) is satisfied within a set tolerance

$$\begin{aligned} ||\underset{f}{T} - \underset{s}{T}|| &< \varepsilon_T \\ ||\underset{f}{q} - \underset{s}{q}|| &< \varepsilon_q \end{aligned} \tag{16}$$

where the tolerances ε_T and ε_q are taken as 0.001.

It should be noted that alternatively the flux could be specified as a boundary condition for the BEM code leading to a flux forward temperature back (FFTB) approach. However, when a fully conjugate solution is undertaken, this would amount to specify second kind boundary conditions completely around the surface of a domain governed by an elliptic equation, resulting in a nonunique solution. The TFFB algorithm avoids such a situation.

3.4 Interpolation between BEM and FVM grids

An issue arises in information transfer between the CFD and the BEM as there exists a significant difference in the levels of discretization between the two meshes in a typical CHT simulation. Accurate resolution of the boundary layer requires a FVM surface grid, which is much too fine to be used directly in the

BEM. A much coarser surface grid is typically generated for the BEM solution of the conduction problem. The disparity between the two grids requires a general interpolation of the surface temperature and heat flux between the two solvers as it is not possible in general to isolate a single BEM node and identify a set of nearest FVM nodes. Indeed in certain regions where the CFD mesh is very fine, a BEM node can readily be surrounded by ten or more FVM nodes.

A distance-weighted interpolation, reminiscent of radial basis function (RBF) interpolation (Partridge *et al.*, 1992), is adopted for the transfer of temperature and flux values between the BEM and the CFD grids. Consider Figure 3(a), where the location of a BEM node is identified on the right-hand side by a star-like symbol. Let us consider the problem of transferring the temperature from the FVM grid to the BEM grid. Let us denote the position of the BEM node of interest by $\vec{r}_i$, and the location of an FVM node by $\vec{r}_j$. The radial distance from every FVM node to the BEM node of interest is then $r_{ij} = |\vec{r}_j - \vec{r}_i|$. Let us suppose that the number of all FVM surface nodes lying within a ball of radius $R_{\max}$ centered about $\vec{r}$ is N_{ball}. Moreover, let us denote two cases. In case I, all $r_{ij} > \varepsilon$ and in case II, there is an FVM node located at $\vec{r}_{j,\varepsilon}$

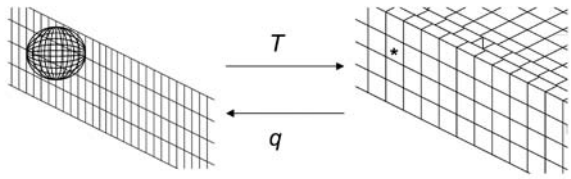

(a) Transfer of nodal temperatures and fluxes between CFD and BEM grids

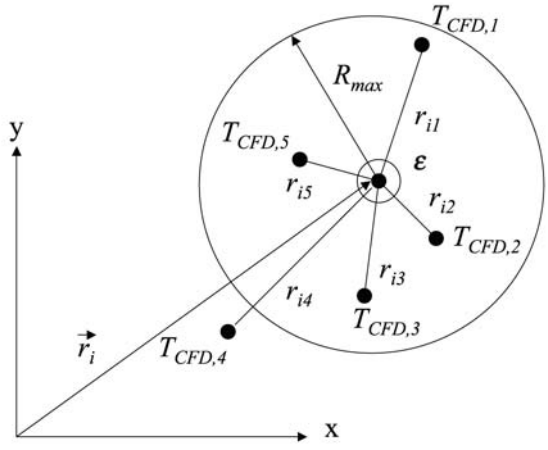

(b) 2-D illustration of five CFD nodes nearest to a BEM node located at $\vec{r}_i$

Figure 3.
Transfer of nodal values from FVM and BEM (and back) independent surface meshes is performed with a distance weighted radial interpolation

such that $r_{ij} \leq \varepsilon$, where ε is a tolerance. Then, the value of the temperature at the BEM node $\vec{r}_j$ is evaluated as

$$T_{\mathrm{BEM}}(\vec{r}_i) = \frac{\sum_{j=1}^{N_{\mathrm{ball}}} \frac{T_{\mathrm{CFD}}(\vec{r}_i)}{r_{ij}}}{\sum_{j=1}^{N_{\mathrm{ball}}} \frac{1}{r_{ij}}} \quad \text{for case I}$$
$$= T_{\mathrm{CFD}}(\vec{r}_{j,\varepsilon}) \quad \text{for case II} \tag{17}$$

In all calculations, the maximum radius $R_{\max}$ of the sphere is set to 2.5 percent of the maximum distance within the solid region and ε is set to $R_{\max} \times 10^{-20}$. These limits may be adjusted to suit the problems at hand.

4. A domain decomposition strategy for BEM models of large-scale three-dimensional heat conduction problems

As mentioned, the BEM is ideally suited for the solution of linear and non-linear heat conduction problems and is particularly a advantageous numerical method due to its boundary-only feature, however, the coefficient matrix of the resulting system of algebraic equations is fully populated. For large-scale 3D problems, this poses very serious numerical challenges due to its large storage requirements and iterative solution of large sets of non-sparse equations. This problem has been approached in the BEM community by one of the two approaches: one is the artificial subsectioning of the 3D model into a multi-region model in conjunction with block-solvers reminiscent of the FEM frontal solvers (Bialecki *et al.*, 1996; Kane *et al.*, 1990) and (2) the adoption of multipole methods in conjunction with the GMRES nonsymmetric iterative solver (Greengard and Strain, 1990; Hackbush and Nowak, 1989). The first approach of domain decomposition (or subsectioning) produces a sparse block coefficient matrix that is efficiently stored and has been successfully implemented in commercial codes such as BETTI and GPBEST in the context of continuous boundary elements. However, the method requires generation of complex data-structures identifying connecting regions and interfaces prior to analysis. The second approach is very efficient, however, it requires complete re-writing of the BEM code to adopt multipole formulation. Recently, a novel technique using wavelet decomposition has been proposed to reduce matrix storage requirements without a need for major alteration of traditional BEM codes (Bucher and Wrobel, 2000).

We propose to adopt the first approach, however, we do not use a block solver but rather a region-by-region iterative solver. Although, it was reported in the literature that this process sometimes has difficulty in converging the non-linear problems (Chima, 1996; Azevedo and Wrobel, 1988), it is shown that

the process converges very efficiently in the linear case and can offer very substantial savings in memory. Moreover, the technique does not require any complex data-structure preparation. Indeed, the approach is somewhat transparent to the user, a significant advantage in coupling the BEM to other field solvers. It should be noted that this subsectioning method is under current development and has not yet been integrated into the CHT solver at the point of writing this paper, and thus the technique along with an example of 3D conduction solution is presented herein with this explicit caveat.

In the standard BEM, if N is the number of boundary nodes used to discretize the problem, the number of floating point operations (FLOPS) required to arrive at the algebraic system is proportional to N^2 as well as direct memory allocation also is proportional to N^2. Enforcing imposed boundary conditions, yields

$$[H]\{T\} = [G]\{q\} \Rightarrow [A]\{x\} = \{b\} \tag{18}$$

where $\{x\}$ contains nodal unknowns T or q, whichever is not specified in the boundary conditions. The solution of the algebraic system for the boundary unknowns can be performed using a direct solution method such as LU decomposition, requiring proportional to N^3 FLOPS or iterative methods such as bi-conjugate gradient or general minimization of residuals that, in general, require FLOPS proportional to N^2 to achieve convergence. In 3D problems of any appreciable size this approach is computationally prohibitive and leads to enormous memory demands.

If a domain decomposition solution process is adopted instead, the domain is decomposed into K subdomains and each one is independently discretized and solved by the standard BEM while enforcing continuity of temperature and heat flux at the interfaces. It is worth mentioning that discretization of neighboring subdomains does not have to be coincident, this is, at the connecting interface, boundary elements and nodes from the two adjoining sub-domains are not required to be structured following a sequence or particular position. The only requirement at the connecting interface is that it forms a closed boundary with the same path on both sides. The information between the neighboring sub-domains separated by an interface can be passed through an interpolation.

The process is shown in two-dimension in Figure 4, with a decomposition four ($K = 4$) subdomains. The boundary value problem is solved independently over each subdomain where initially, a guessed boundary condition is imposed over the interfaces in order to ensure the well-posedness of each subproblem. The problem in subdomain Ω_1 is transformed into

$$\nabla^2 T_{\Omega_1}(x,y) = 0 \Rightarrow [H_{\Omega_1}]\{T_{\Omega_1}\} = [G_{\Omega_1}]\{q_{\Omega_1}\} \tag{19}$$

The composition of this algebraic system requires (n^2) FLOPS where n is the number of boundary nodes in the subdomain as well as (n^2) for direct memory

allocation. This new proportionality number n is roughly equivalent to $n \approx 2N/K + 1$, as long as the discretization along the interfaces has the same level of resolution as the discretization along the boundaries. Direct memory allocation requirement for later algebraic manipulation is now reduced to a proportion of n^2 as the influence coefficient matrices can easily be stored in ROM memory for later use after the boundary value problems on remaining subdomains have been effectively solved. For the example shown here, where the number of subdomains is $K = 4$, the new proportionality value n is approximately equal to $n \approx 2N/5$. This simple multi-region example reduces the memory requirements to about $n^2/N^2 = (4/25) = 16$ percent of the standard BEM approach.

The algebraic system for subdomain Ω_1 is re-arranged, with the aid of given and guessed boundary conditions, as:

$$[H_{\Omega_1}]\{T_{\Omega_1}\} = [G_{\Omega_1}]\{q_{\Omega_1}\} \Rightarrow [A_{\Omega_1}]\{x_{\Omega_1}\} = \{b_{\Omega_1}\} \tag{20}$$

Now, the solution of the new algebraic system of subdomain Ω_1 requires a number FLOPS proportional to $n^3/N^3 = (8/125) = 6.4$ percent of the standard BEM approach if a direct algebraic solution method is employed, or a number of FLOPS proportional to $n^2/N^2 = (4/25) = 16$ percent of the standard BEM approach if an indirect algebraic solution method is employed. For both, FLOPS count and direct memory requirement, the reduction is dramatic. However, as the first set of solutions for the subdomains were obtained using guessed boundary conditions along the interfaces, the global solution needs to follow an iteration process and satisfy a convergence criteria.

Globally, the FLOPS count for the formation of the algebraic setup for all K subdomains must be multiplied by K, therefore, the total operation count for the coefficient matrices computation is given by: $Kn^2/N^2 \approx 4K/(K+1)^2$. For this particular case with $K = 4$, $Kn^2/N^2 = 16/25 = 64$ percent of the standard BEM approach. Moreover, the more significant reduction is revealed in the RAM memory requirements as only the memory needs for one of the subdomains must be allocated at a time. The rest of the coefficient matrices for the remaining subdomains can be temporarily stored in ROM memory until access and manipulation is required or if a parallel strategy is adopted the matrices for each subdomain are stored by its assigned processor. Therefore, for this case of $K = 4$, the true memory reduction is $n^2/N^2 = 4/25 = 16$ percent of the standard BEM.

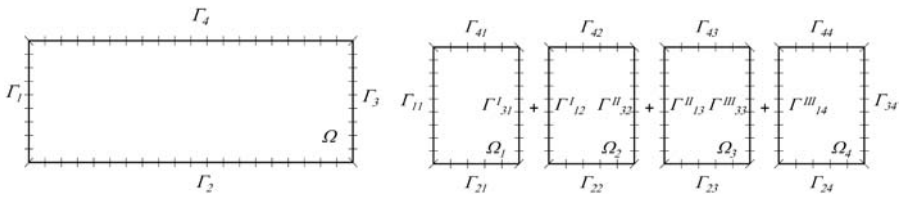

Figure 4.
BEM single region discretization and four domain BEM decomposition

With respect to the algebraic solution of the system of equation (20), if a direct approach as the LU factorization is employed for all subdomains, the LU factors of the coefficient matrices for all subdomains can be computed only once at the first iteration step and stored in ROM memory, or on disc, for later use during the iteration process for which only a forward and a backward substitution will be required. This feature allows a significant reduction in the operational count through the iteration process until convergence is achieved, as only a number of floating point operations proportional to n as opposed to n^3 is required at each iteration step. To this computation time the access to ROM memory is added at each iteration step, which is usually larger than access to RAM. Alternatively, if the overall convergence of the problem requires few iterations, iterative solvers such as GMRES offer an efficient alternative.

Providing a good initial guess is crucial to the success of any iteration. To this end, first we typically solve the problem using a coarse grid constant model (Figure 2) obtained by collapsing the nodes of the discontinuous bilinear element to the centroid, and supply that model with a physically-based initial guess for interface temperatures. An efficient initial guess can be made using a physically based 1D heat conduction argument for every node on the external surfaces to every node at the interface. The initial guess for any interfacial node is provided algebraically as:

$$T_i = \frac{\displaystyle\sum_{j=1}^{N_T} B_{ij} T_j - \sum_{j=1}^{N_q} B_{ij} R_{ij} q_j + \sum_{j=1}^{N_h} \frac{B_{ij} H_{ij} T_{\infty j}}{H_{ij}+1}}{\displaystyle S_i - \sum_{j=1}^{N_T} B_{ij} + \sum_{j=1}^{N_h} \frac{B_{ij} H_{ij}}{H_{ij}+1}} \tag{21}$$

where N_T, N_q, and N_h are the number of first, second, and third kind boundary conditions specified at the external (non-interfacial) surfaces and

$$B_{ij} = \frac{A_j}{|r_{ij}|}, \qquad R_{ij} = \frac{\vec{r}_{ij} \cdot \hat{n}_j}{k}, \qquad H_{ij} = \frac{h_j}{k}(\vec{r}_{ij} \cdot \hat{n}_j), \qquad S_i = \sum_{j=1}^{N} \frac{A_j}{|r_{ij}|} \tag{22}$$

with $N = N_T + N_q + N_h$, the thermal conductivity of the medium is k, the film coefficient at the j-th convective surface is h_j, the outward-drawn normal to any surface is $\hat{n}_j$, the position vector from the interfacial node i to the external surface node j is $\vec{r}_{ij}$ and its magnitude is $r_{ij} = |\vec{r}_{ij}|$, while the area of element j denoted is readily computed as:

$$A_j = \oint_{\Gamma_j} \mathrm{d}\Gamma(x,y,z) = \int_{-1}^{+1}\int_{-1}^{+1} |J_j(\eta,\zeta)|\,\mathrm{d}\eta\,\mathrm{d}\zeta.$$

Once the initial temperatures are imposed as boundary conditions at the interfaces, a resulting set of normal heat fluxes along the interfaces will be computed. These are then non-symmetrically averaged in an effort to match the heat flux from neighboring subdomains. Considering a two-domain substructure, the non-symmetric averaging at the interface is explicitly given as,

$$q^I_{\Omega_1} = q^I_{\Omega_1} - \frac{q^I_{\Omega_1} + q^I_{\Omega_2}}{2} \qquad \text{and} \qquad q^I_{\Omega_2} = q^I_{\Omega_2} - \frac{q^I_{\Omega_2} + q^I_{\Omega_1}}{2} \tag{23}$$

to ensure the flux continuity condition $q^I_{\Omega_1} = -q^I_{\Omega_2}$ after averaging. Compactly supported radial basis interpolation can be employed for the flux average to account for the unstructured grids along the interface from neighboring subdomains.

Using these fluxes, the BEM equations are again solved leading to mismatched temperatures along the interfaces for neighboring subdomains. These temperatures are interpolated, if necessary, from one side of the interface to the other side using a compactly supported radial basis functions to account for the possibility of interface mismatch between the adjoining substructure grids. Once this is accomplished, the temperature is averaged out at each interface. Illustrating this for a two-domain substructure, again we have for regions 1 and 2 interfaces,

$$T^I_{\Omega_1} = \frac{T^I_{\Omega_1} + T^I_{\Omega_2}}{2} + R'' q^I_{\Omega_1} \qquad \text{and} \qquad T^I_{\Omega_2} = \frac{T^I_{\Omega_1} + T^I_{\Omega_2}}{2} + R'' q^I_{\Omega_2} \tag{24}$$

in general, to account for a case where a physical interface exists and a thermal contact resistance is present between the connecting subdomains, where R'' is the thermal contact resistance imposing a jump on the interface temperature values. These now matched temperatures along the interfaces are used as the next set of boundary conditions.

The iteration process is continued until a convergence criterion is satisfied. A measure of convergence may be defined as the L_2 norm of mismatched temperatures along all interfaces as:

$$L_2 = \sqrt{\frac{1}{K \cdot N^I} \sum_{k=1}^{K} \sum_{i=1}^{N^I} (T^I - T^I_u)^2} \tag{25}$$

This norm measures the standard deviation of BEM computed interface temperatures T^I and averaged-out updated interface temperatures T^I_u. The iteration routine can be stopped once this standard deviation reaches a small fraction ε of $\Delta T_{\max}$, where $\Delta T_{\max}$ is the maximum temperature span of the global field. It is noted, that we refer to an iteration as the process by which an iterative sweep is carried out to update both the interfacial fluxes and

temperatures such that the above norm may be computed. We set $\varepsilon = 5 \times 10^{-3}$ in our computations.

5. Numerical results and discussion

We now present results of a full conjugate solution of a film-cooled blade under operating conditions, which match a planned experiment at NASA Glenn Research center and assumes periodicity in the spanwise direction for one pitch of film-cooling hole patterns. We compare results of this simulation to those obtained from the standard two temperature method. This simulation uses the standard BEM approach to heat conduction. We also present results from a heat conduction simulation for a cooled turbine vane using the subsectioning method described in this paper.

5.1 CHT simulation of a 3D film-cooled turbine blade

Film cooling is commonly used in turbine designs to produce a buffer layer of relatively cool air between the turbine blade and the hot freestream gas in the first and second rows of blades and vanes. The CHT computation is carried out on a computational model of a realistic film-cooled turbine vane according to the three-dimensional vane geometry including plena and film holes and is based on a Honeywell film-cooled engine design, (Heidmann *et al.*, 2002). The geometry of this test vane is based on the engine vane midspan coordinates, and is scaled up by a factor of 2.943 to allow matching of engine exit Mach number (0.876) and exit Reynolds number (2.9×10^6 based on true chord) with atmospheric inlet conditions. The test vane has a true chord of 0.206 m. Since the test vane is of constant cross-section, only one spanwise pitch of the film hole pattern was discretized, with periodicity of the flow-field enforced at each end. This simplification assumes no effect of endwalls, but greatly reduces the number of grid points required to model the vane. However, the thermal boundary conditions enforced at these ends in the conduction analysis were adiabatic. The vane has two plena, which feed 12 rows of film cooling holes as well as trailing-edge ejection slots, (Figure 5). Trailing edge ejection is blocked in the computation as the planned experiment has no slot cooling. Detailed geometrical data for each row of film holes as well as hole distribution are provided in Heidmann *et al.* (2002). A multi-block grid approach is adopted to model this complex geometry and generated the FVM grid using the topology-based algebraic grid-generation program GridPro™ (Program Development Corporation, 1997) with the final grid consisting of 140 blocks and a total of 1.2×10^6 finite volume computational cells. The FVM grid consists of 20 cells across both the inlet and outlet boundaries, 60 cells on the periodic boundary, over 200 cells around the vane, and 44 cells from the vane to the periodic boundary.

A blade-to-blade view of the FVM grid is shown in Figure 6. Figure 7 shows the FVM grid in the leading edge region of the vane.

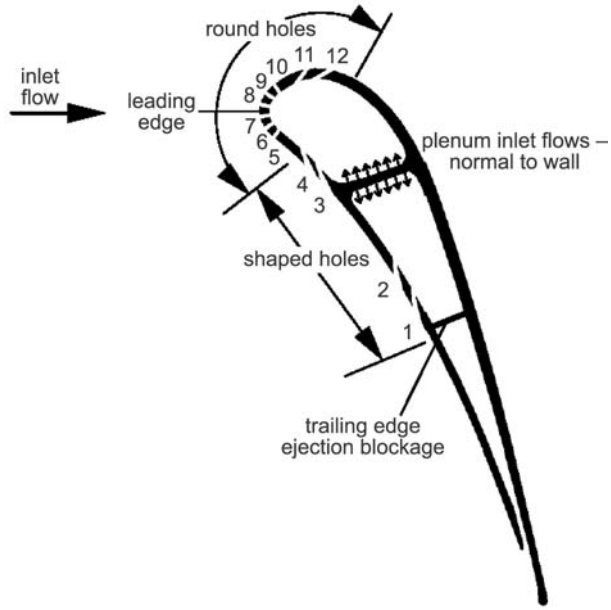

Figure 5.
Film-cooled blade profile used in the CHT simulation

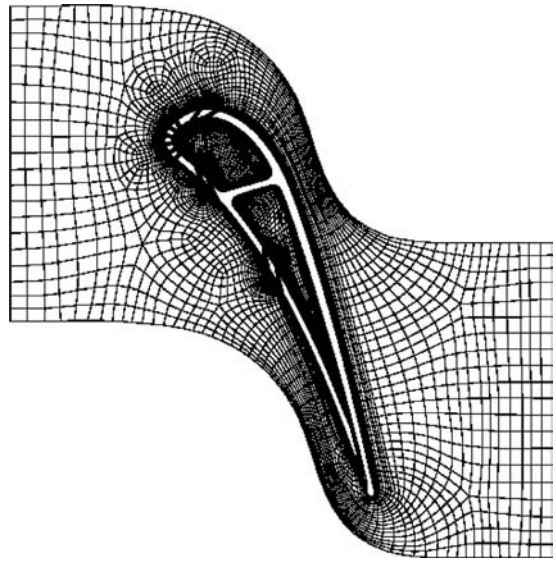

Figure 6.
Blade-to-blade computational grid cross-section

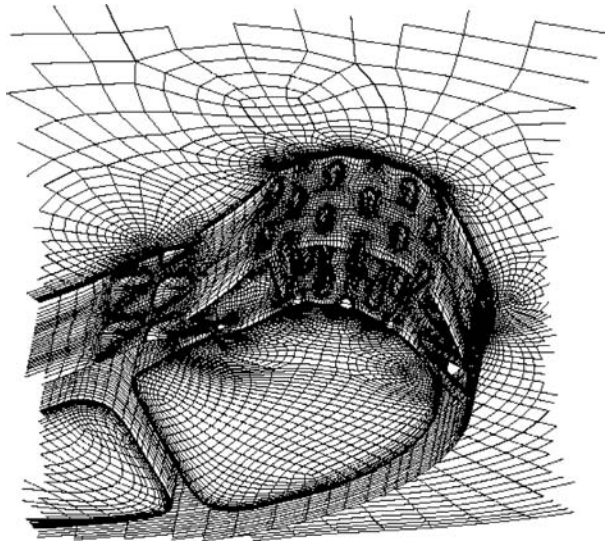

Figure 7.
FVM grid in the leading edge region of the blade

The flow conditions for all simulations use a free-stream inlet flow to the vane at an angle of 0° to the axial direction, with all temperatures and pressures normalized by the inlet stagnation values of 3,109 R and 10 atmospheres, respectively. The inlet turbulence intensity is set at 8.0 percent and the turbulence scale is 15.0 percent of vane true chord. Other inflow quantities are set by means of the upstream-running Riemann invariant. The vane downstream exit flow is defined by imposing a constant normalized static pressure of 0.576, which was empirically determined to yield a desired exit Mach number of 0.876. Periodicity was enforced in both the blade-to-blade and spanwise directions based on vane and film hole pitches, respectively. Moreover, in order to maintain a true periodic solution, inflow to the plena was provided by defining a region of each plenum wall as an inlet and introducing uniform flow normal to the wall. In Figure 6, these regions are shown to lie on either side of the internal wall that separates the two plena. In practice, there will be spanwise flow in the plenum, but bleed of the plenum flow into the film holes results in a spanwise-varying mass flow rate and static pressure, which would violate spanwise periodicity imposed in this particular reduced computational model. The non-dimensionalized inflow stagnation temperature to the plena was 0.5, corresponding to a coolant temperature of 1554.5 R. The velocity was fixed to the constant value required to provide the design mass flow rate to each plenum, and static pressure was extrapolated from the interior. The inflow patch for each plenum was defined to be sufficiently large to yield very low inlet velocities (Mach number < 0.05), allowing each plenum to approximate an ideal plenum. All solid walls were imposed with a no-slip

boundary condition. The blade metal material is taken as Inconel with a conductivity of $k_{\text{blade}} = 1.34$ Btu/h in R taken at 2174.9 R which is estimated to be the average blade temperature.

The FVM metal surface grid consists of 38,000 cells at the 4th level of multi-grid. The grid was coarsened to generate a BEM grid of 13,000 bilinear cells with 52,000 nodal unknowns. Two cases are computed in the numerical simulation in order to obtain the metal temperature:

(1) The traditional two-temperature approach, whereby two different isothermal wall boundary conditions extended to all wall surfaces, including the film hole surfaces and plenum surfaces. Two solutions were generated with constant wall temperatures T_{w} of $T_{\text{w},1} = 2174.9\,\text{R}$ and $T_{\text{w},2} = 2485.6\,\text{R}$ imposed on all blade surfaces. The flow-field was computed from the plena through the cooling holes and over the blade. The predicted wall heat fluxes at each node q''_{w} computed from each of these isothermal solutions were used to simultaneously solve adiabatic wall temperature, T_{aw}, and heat transfer coefficient, h, referenced to the computed adiabatic wall temperature, under the assumption that T_{aw} and h are independent of the wall temperature. That is at each node we have

$$\begin{aligned} q''_{\text{w}} &= h(T_{\text{w},1} - T_{\text{aw}}) \\ q''_{\text{w}} &= h(T_{\text{w},2} - T_{\text{aw}}) \end{aligned} \tag{26}$$

In turn, these film coefficient and associated adiabatic wall distributions were used in the BEM to compute metal temperatures.

(2) A full CHT solution was carried out using the same grids and boundary conditions as above except at the blade surface where conjugate conditions were imposed. The conjugate solutions converged in 1,000 iterations with a BEM conduction calculation performed each ten FVM iterations. The BEM code was written as a subroutine to the Glenn-HT code and subroutines were coded to exchange information between the two codes in terms of the FVM and BEM grids as well as boundary condition information. The Glenn-HT code was modified to allow non-isothermal boundary condition specification.

All computations were performed at NASA Glenn Research Center on an SGI Origin 2000 cluster with 32 processors. Flow computations were carried out and considered converged when residuals were driven below 10^{-5}. Results of the blade surface temperatures predicted by the simulations are shown in Figure 8 for the CHT solution and in Figure 9 for the two constant temperature approaches. The two temperature distributions are markedly different with a temperature span of $\Delta T = 1720 - 2420\,\text{R}$ across the surface of the blade while the CHT solution predicted a temperature span of $\Delta T = 1620 - 2620\,\text{R}$ across the blade. In addition to CHT computations predicting lower minimum (100 R colder) and higher maximum temperatures (200 R hotter), the distribution of cold and hot regions are quite different as is evident from the surface plots.

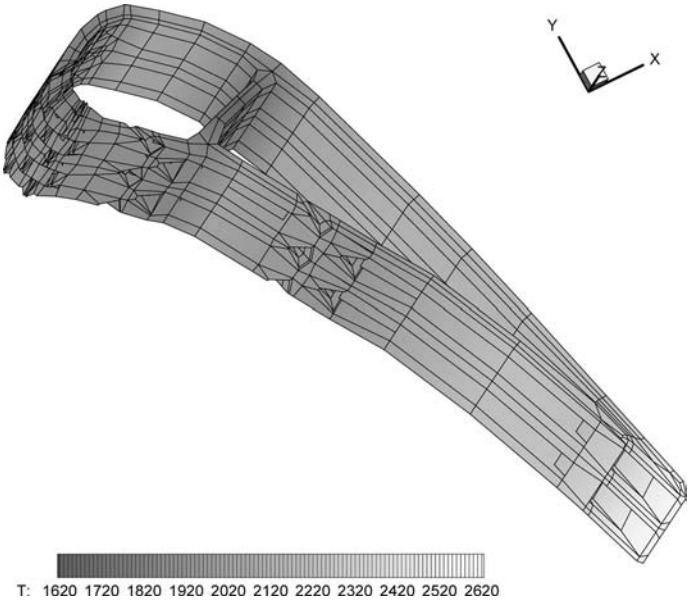

Figure 8.
Blade surface temperature predicted by the CHT solution

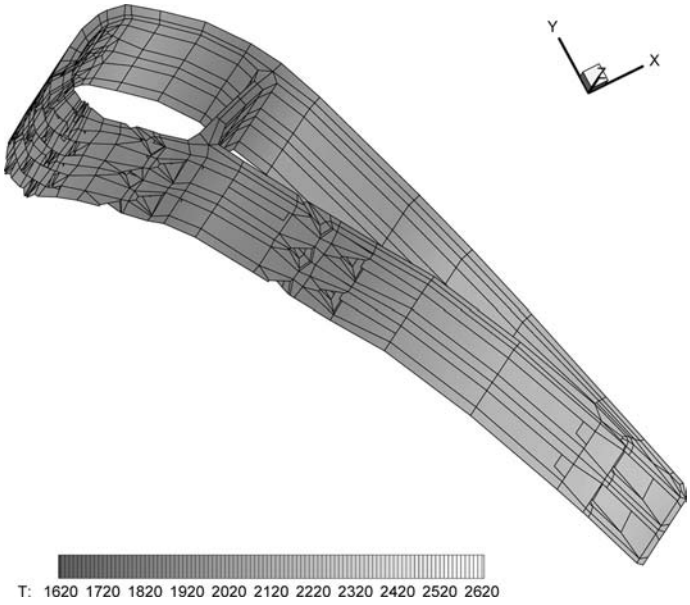

Figure 9.
Blade surface temperature predicted by the BEM using h and T_{aw} provided from the two-temperature approach

For instance, with conduction taken into consideration in the CHT simulation, the thin trailing regions are seen to reach higher temperatures than predicted by the isothermal approach, while the forward plenum region is seen to be effectively cooler. This has severe implications in materials design and subsequent thermal stress analysis of the blade carried out using these metal temperatures.

Results are now presented for a simulation using the subsectioning iterative method for a pure heat conduction problem. Here, a blade with a 10 cm chord and 14 cm in the spanwise direction is taken. The blade is cooled by two plena (Figure 10). The blade is discretized using GridPro^{TM} (Program Development Corporation, 1997) into six subsections with a surface grid of a total of nearly 6,000 bilinear elements or nearly 24,000 degrees of freedom (Figure 11). Each block is kept at a discretization level nearer to 1,000 bilinear boundary elements. Adiabatic conditions are imposed on the top and bottom surfaces of the blade. Convective boundary conditions are imposed on all other surfaces. The film coefficient on the outer surface of the blade is taken as $h = 1,000\,\mathrm{W/m^2K}$ with the reference temperature taken as 1,000 K, while the cooling plena are both imposed with film coefficients $h = 500\,\mathrm{W/m^2K}$ with the reference temperature taken as linearly varying from 300 K to 400 K in the increasing z-direction of the cooling plenum closest to the leading edge, while

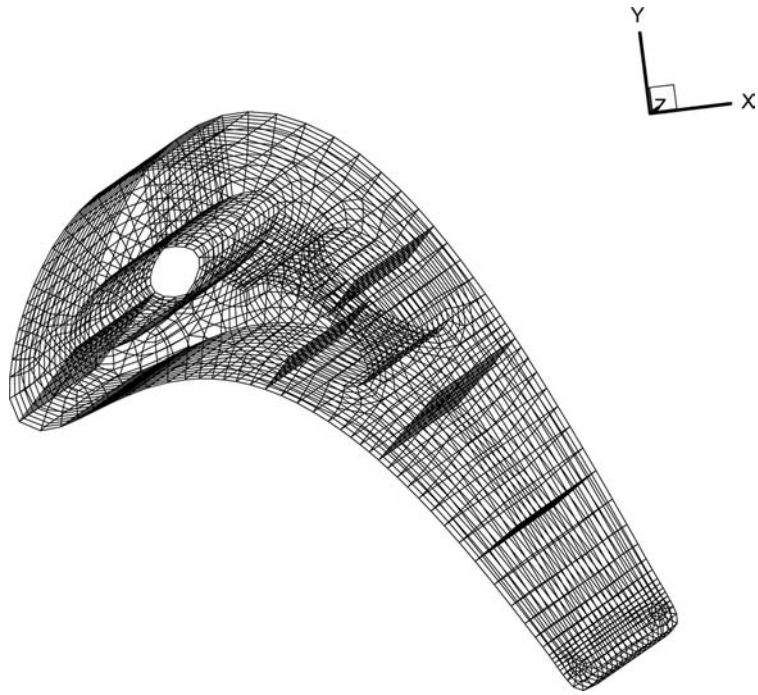

Figure 10.
BEM grid for 3D cooled blade

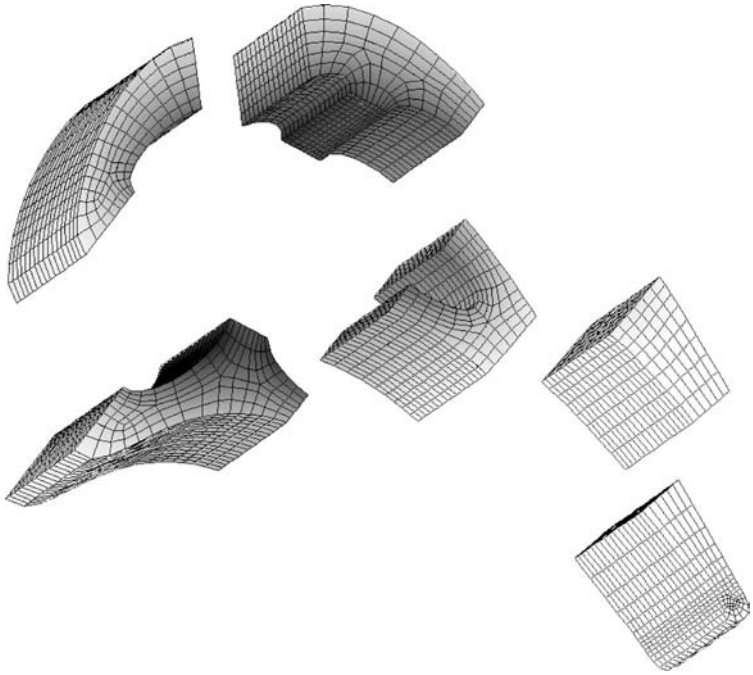

Figure 11.
Domain decomposition of a 3D plenum-cooled turbine blade

linearly varying from 500 K to 400 K in the decreasing z-direction of the cooling plenum closest to the trailing edge.

All computations were performed on a Pentium 4, 1.8 GHz PC with 512 MB 800 MHz RDRAM. The initial guess using equation (21) alone without the coarse grid model provided an excellent starting point for the iteration, which converged on 8 steps to provide an L_2 iterative norm, defined in equation (25), of 0.00011698. It took 34,905 s to set up the matrices, obtain and store their LU factors, and 813 s to solve the problem iteratively. The resulting temperature plots shown in Figures 11 and 12 reveal a very smooth distribution across all blocks. The resulting surface heat fluxes are presented in Figure 13 revealing a very smooth distribution from a minimum of $-180{,}000\ W/m^2K$ to a maximum of $230{,}000\ W/m^2K$. It should be noted that the subsectioning approach is ideally suited for parallel implementation. The authors are pursuing this avenue prior to integration of the algorithm with the CHT solver. This concludes the example section.

6. Conclusions

A combined BEM/FVM approach using the TFFB conjugate method has been implemented in a 3D context to model CHT in cooled turbine blades. As a

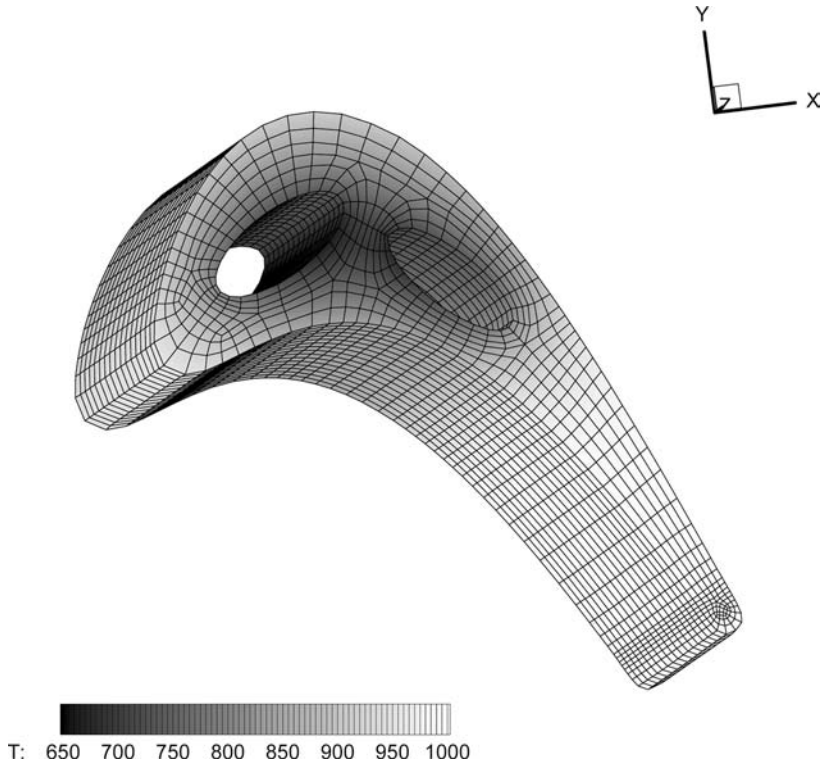

Figure 12.
Converged surface temperature distribution (*K*)

boundary-only grid is used by the BEM, the computational time for the heat conduction analysis is insignificant compared to the time used for the NS analysis. The proposed method produces realistic results without using arbitrary assumptions for the thermal condition at the conductor surface. Results from a CHT numerical simulation of a 3D film-cooled blade section are presented and are compared with those obtained from the standard approach of a two temperature model. A significant difference in the level and distribution of the metal temperatures is found between the two models. These differences have severe implications in materials design and subsequent thermal stress analysis of the blade carried out using these metal temperatures. In practice, turbomachinery components such as modern cooled turbine blades often contain several hundred film cooling holes and intricate internal serpentine cooling passages with complex convective enhancement configurations such as turbulating trip strips. This poses a real computational challenge to BEM modeling. The subsectioning iterative approach outlined in this paper offers promising technique to address this problem. It is proposed to extend the current work by implementing the parallel implementation of iterative domain

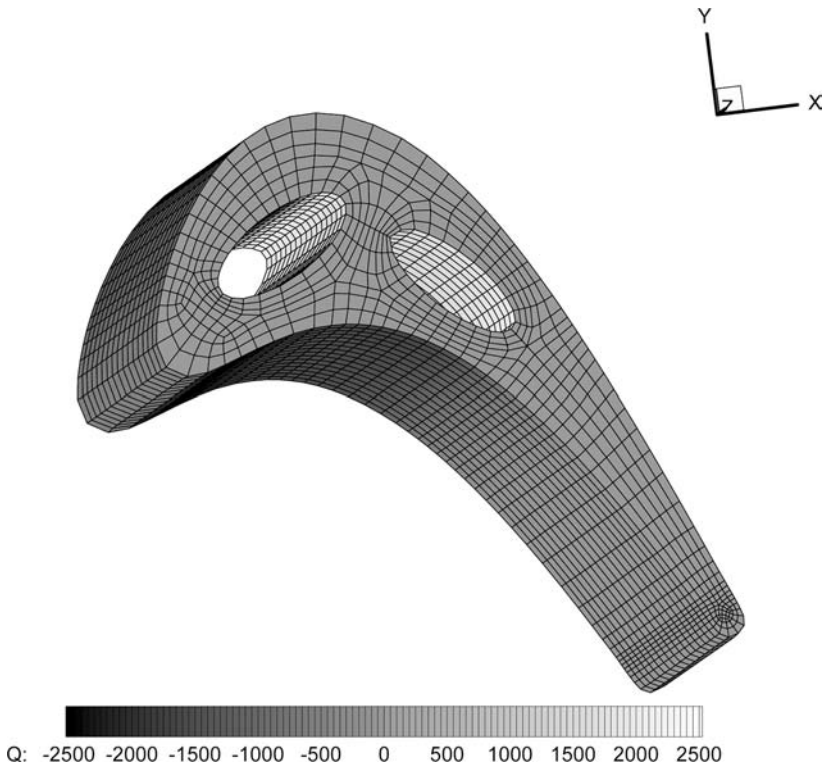

Figure 13.
Converged surface heat flux distribution ($1/100\ W/m^2K$)

decomposition approach for the BEM in order to address large-scale CHT problems and results of such simulations will soon be reported elsewhere (Divo *et al.*, 2003; Heidmann *et al.*, 2003).

References

Ameri, A.A., Steinthorsson, E. and Rigby, D.L. (1997), "Effect of squealer tip on rotor heat transfer and efficiency", *ASME Paper 97-GT-128*.

Azevedo, J.P.S. and Wrobel, L.C. (1988), "Non-linear heat conduction in composite bodies: a boundary element formulation", *International Journal for Numerical Methods in Engineering*, Vol. 26, pp. 19-38.

Banerjee, P.K. (1994), *Boundary Element Method*, McGraw-Hill, NY, USA.

Bialecki, R. and Nhalik, R. (1989), "Solving nonlinear steady state potential problems in inhomogeneous bodies using the boundary element method", *Numerical Heat Transfer, Part B*, Vol. 15, pp. 79-96.

Bialecki, R.A., Merkel, M., Mews, H. and Kuhn, G. (1996), "In-and out-of-core BEM equation solver with parallel and nonlinear options", *International Journal for numerical Methods in Engineering*, Vol. 39, pp. 4215-42.

Bialecki, R., Ostrowski, Z., Kassab, A., Qi, Y. and Sciubba, E. (2001), "Coupling finite element and boundary element solutions", *Proc. of the 2001 European Conference on Computational Mechanics*, 26-29 June, 2001, Cracow, Poland.

Bohn, D.E., Becker, V.J. and Rungen, A.U. (1997), "Experimental and numerical conjugate flow and heat transfer investigation of a shower-head cooled turbine guide vane", *ASME Paper 97-GT-15*.

Bohn, D., Becker, V., Kusterer, K., Otsuki, Y., Sugimoto, T. and Tanaka, R. (1999), "3-D internal conjugate calculations of a convectively cooled turbine blade with serpentine-shaped ribbed channels", *IGTI Paper 99-GT-220*.

Brebbia, C.A. and Dominguez, J. (1989), *Boundary Elements: An Introductory Course*, Computational Mechanics Pub., Southampton and McGraw-Hill, NY, USA.

Brebbia, C.A., Telles, J.C.F. and Wrobel, L.C. (1984), *Boundary Element Techniques*, Springer-Verlag, Berlin.

Brown, S.A. (1997), "Displacement extrapolations for CFD+CSM aeroelastic analysis", *AIAA Paper 97-1090*

Bucher, H. and Wrobel, L.C. (2000), "A novel approach to applying wavelet transforms in boundary element method", in Denda, M., Aliabadi, M.H. and Charafi, A. (Eds), *Advances in Boundary Element Techniques,* II, Hogaar Press, Switzerland, pp. 3-11.

Chima, R.V. (1996), "A k-ω turbulence model for quasi-dimensional turbomachinery flows", *NASA TM-107051*.

Comini, G., Saro, O. and Manzan, M. (1993), "A physical approach to finite element modeling of coupled conduction and convection", *Numerical Heat Transfer, Part B*, Vol. 24, pp. 243-61.

Divo, E.A., Kassab, A.J. and Rodriguez, F. (2003), "Domain decomposition for 3D boundary elements in non-linear heat conduction", *ASME Paper HT2003-40553*.

Dowell, E. and Hall, K.C. (2001), "Modeling of fluid structure interaction", *Annual Review of Fluid Mechanics*, Vol. 33, pp. 445-90.

Greengard, L. and Strain, J. (1990), "A fast algorithm for the evaluation of heat potentials", *Communications in Pure and Applied Mathematics*, Vol. 43, pp. 949-63.

Hackbush, W. and Nowak, Z.P. (1989), "On the fast multiplication in the boundary element method by panel clustering", *Numerische Mathematik*, Vol. 54, pp. 463-91.

Hahn, Z., Dennis, B. and Dulikravich, G. (2000), "Simultaneous prediction of external flow-field and temperature in internally cooled 3-D turbine blode material", *IGTI Paper 2000-GT-253*.

Hassan, B., Kuntz, D. and Potter, D.L. (1998), "Coupled fluid/thermal prediction of ablating hypersonic vehicles", *AIAA Paper 98-0168*.

He, M., Bishop, P., Kassab, A.J. and Minardi, A. (1995a), "A coupled FDM/BEM solution for the conjugate heat transfer problem", *Numerical Heat Transfer, Part B: Fundamentals*, Vol. 28 No. 2, pp. 139-54.

He, M., Kassab, A.J., Bishop, P.J. and Minardi, A. (1995b), "A coupled FDM/BEM iterative solution for the conjugate heat transfer problem in thick-walled channels: constant temperature imposed at the outer channel wall", *Engineering Analysis*, Vol. 15 No. 1, pp. 43-50.

Heidmann, J., Rigby, D. and Ameri, A. (2002), "A three-dimensional coupled external/internal simulation of a film-cooled turbine vane", *ASME Journal of Turbomachinery*, Vol. 122, pp. 348-59.

Heidmann, J.D., Kassab, A.J., Divo, E.A., Rodriguez, F. and Steinthorsson, E. (2003), "Conjugate heat transfer effects on a realistic film-cooled turbine vane", *ASME Paper GT2003-G38553*.

Jameson, A., Schmidt, W. and Turkel, E. (1981), "Numerical simulation of the Euler equations by the finite volume methods using Runge-Kutta time stepping schemes", *AIAA Paper 81-1259*.

Kane, J. (1994), *Boundary Element Analysis in Engineering and Continuum Mechanics*, Prentice-Hall, Englewood Cliffs, New Jersey.

Kane, J.H., Kashava-Kumar, B.L. and Saigal, S. (1990), "An arbitrary condensing, noncondensing strategy for large scale, multi-zone boundary element analysis", *Computer Methods in Applied Mechanics and Engineering*, Vol. 79, pp. 219-44.

Kao, K.H. and Liou, M.S. (1997), "Application of chimera/unstructured hybrid grids for conjugate heat transfer", *AIAA Journal*, Vol. 35 No. 9, pp. 1472-8.

Kassab, A.J. and Aliabadi, M.H. (Eds) (2001), *Advances in Boundary Elements: Coupled Field Problems*, Computational Mechanics, Boston.

Kassab, A.J. and Nordlund, R.S. (1994), "Addressing the corner problem in the BEM solution of heat conduction problems", *Communications in Numerical Methods in Engineering*, Vol. 10, pp. 385-92.

Kassab, A.J. and Wrobel, L.C. (2000), "Boundary element methods in heat conduction", in Mincowycz, W.J. and Sparrow, E.M. (Eds), *Recent Advances in Numerical Heat Transfer,* Chapter 5, Taylor and Francis, New York, Vol. 2, pp. 143-88.

Kellogg, O.D. (1953), *Foundations of Potential Theory*, Dover, New York.

Kontinos, D. (1997), "Coupled thermal analysis method with application to metallic thermal protection panels", *AIAA Journal of Thermophysics and Heat Transfer*, Vol. 11 No. 2, pp. 173-81.

Li, H. and Kassab, A.J. (1994a), "Numerical prediction of fluid flow and heat transfer in turbine blades with internal cooling", *AIAA/ASME Paper 94-2933*.

Li, H. and Kassab, A.J. (1994b), "A coupled FVM/BEM solution to conjugate heat transfer in turbine blades", *AIAA Paper 94-1981*.

Liggett, J.A. and Liu, P.L.-F. (1983), *The Boundary Integral Equation Method for Porous Media Flow*, Allen and Unwin, Boston.

Menter, F.R. (1993), "Zonal two-equation k-ω turbulence models for aerodynamic flows", *AIAA Paper 93-2906*.

Morse, P.M. and Feshbach, H. (1953), *Methods of Theoretical Physics*, McGraw-Hill, NY, USA.

Partridge, P.W., Brebbia, C.A. and Wrobel, L.C. (1992), *The Dual Reciprocity Boundary Element Method*, Computational Mechanics Publications, Southampton.

Patankar, S.V. (1978), "A numerical method for conduction in composite materials, flow in irregular geometries and conjugate heat transfer", *Proc. 6th. Int. Heat Transfer Conf.*, NRC Canada, and Hemisphere Pub. Co., New York, Vol. 3, pp. 297-302

Program Development Corporation (1997), GridPro™/az3000-User's guide and reference manual, White Plains, New York.

Rahaim, C., Cavalleri, R.J. and Kassab, A.J. (1997), "Computational code for conjugate heat transfer problems an experimental validation effort", *AIAA Paper 97-2487*.

Rahaim, C.P., Kassab, A.J. and Cavalleri, R. (2000), "A coupled dual reciprocity boundary element/finite volume method for transient conjugate heat transfer", *AIAA Journal of Thermophysics and Heat Transfer*, Vol. 14 No. 1, pp. 27-38.

Rigby, D.L., Ameri, A.A. and Steinthorsson, E. (1997), "Numerical prediction of heat transfer in a channel with ribs and bleed", *ASME Paper 97-GT-431*.

Schlichting, H. (1979), *Boundary Layer Theory*, 7th edition, McGraw-Hill, NY, USA, pp. 312-13.

Shyy, W. and Burke, J. (1994), "Study of iterative characteristics of convective diffusive and conjugate heat transfer problems", *Numerical Heat Transfer, Part B*, Vol. 26, pp. 21-37.

Steinthorsson, E., Ameri, A. and Rigby, D. (n.d.), *LeRC-HT-The NASA Lewis Research Center General Multi-Block Navier-Stokes Convective Heat Transfer Code*, (unpublished).

Steinthorsson, E., Liou, M.-S. and Povinelli L.A. (1993), "Development of an explicit multi-block/multigrid flow solver for viscous flows in complex geometries", *AIAA Paper 93-2380*.

Tayala, S.S., Rajadas, J.N. and Chattopadyay, A. (2000), "Multidisciplinary optimization for gas turbine airfoil design", *Inverse Problems in Engineering*, Vol. 8 No. 3, pp. 283-307.

Turkel, E. (1987), "Preconditioned methods for solving the incompressible and low-speed compressible equations", *Journal of Computational Physics*, Vol. 72 No. 2, pp. 277-98.

Turkel, E. (1993), "Review of preconditioning methods for fluid dynamics", *Applied Numerical Mathematics*, Vol. 12, pp. 257-84.

Wilcox, D.C. (1993), Turbulence Modeling for CFD, DCW Industries, La Canada, California.

Wilcox, D.C. (1994), "Simulation of transition with a two-equation turbulence model", *AIAA Journal*, Vol. 32 No. 2, pp. 247-55.

Ye, R., Kassab, A.J. and Li, H.J. (1998), "FVM/BEM approach for the solution of nonlinear conjugate heat transfer problems", in Kassab, A.J., Brebbia, C.A. and Chopra, M.B. (Eds) *Proc. BEM 20*, 19-21 August, Orlando, Florida, pp. 679-89.

Further reading

Abramowitz, M. and Stegun, I. (1965), *Handbook of Mathematical Functions*, Dover Publications, New York.

Divo, E., Rodriguez, F. and Kassab, A.J. (n.d.), "A strategy for linear and nonlinear three dimensional BEM heat conduction models", *Numerical Heat Transfer* (in review).

Ralston, A. and Rabinowitz, P. (1978), *A First Course in Numerical Analysis*, McGraw-Hill, NY, USA.